

Multiple holographic optical tweezers parallel calibration with optical potential well characterization

Federico Belloni, Serge Monneret, Fabien Monduc, and Maxime Scordia

Institut Fresnel, Domaine Universitaire de St. Jerome, 13397 Marseille, France

CIML, CNRS, Institut National de la Sant et de la Recherche Mdicale, Parc Scientifique de Luminy, Case 906, 13009 Marseille, France

federico.belloni@fresnel.fr

<http://www.fresnel.fr/mosaic>

Abstract: We report the extension to a multi-axes exploration of the potential well reconstruction method against drag force to simultaneously characterize the potential wells of several trapping sites generated with holographic optical tweezers. The final result is a robust, fast and automatic procedure we use to characterize holographic tweezers. We mainly focus on the reliability of the method and its application to address the dependence of the diffraction efficiency with the trap position in a given holographic traps pattern.

© 2008 Optical Society of America

OCIS codes: (140.7010) Laser trapping; (350.4855) Optical tweezers or optical manipulation

References and links

1. P. N. Lebedev, "Experimental examination of light pressure," *Annalen der Physik* **6**, 433 (1901).
2. A. Ashkin, J. M. Dziedzic, J. E. Bjorkholm, and S. Chu, "Observation of a single-beam gradient force optical trap for dielectric particles," *Opt. Lett.* **11**, 288–290 (1986).
3. G. Lenormand, S. Henon, A. Richert, J. Simeon, and F. Gallet, "Direct measurement of the area expansion and shear moduli of the human red blood cell membrane skeleton," *Biophys. J.* **81**, 43–56 (2001).
4. K. Svoboda and S. M. Block, "Force and velocity measured for single kinesin molecules," *Cell* **77**, 773–784 (1994).
5. R. M. Simmons, J. T. Finer, S. Chu, and J. A. Spudich, "Quantitative measurements of force and displacement using an optical trap," *Biophys. J.* **70**, 1813–1822 (1996).
6. J. C. Meiners and S. R. Quake, "Femtonewton force spectroscopy of single extended dna molecules," *Phys. Rev. Lett.* **84**, 5014–5017 (2000).
7. M. Polin, K. Ladavac, S.-H. Lee, Y. Roichman and D. Grier, "Optimized holographic optical traps," *Opt. Express* **13**, 5831–5845 (2005).
8. N. Malagnino, G. Pesce, A. Sasso, and E. Arimondo, "Measurements of trapping efficiency and stiffness in optical tweezers," *Opt. Commun.* **214**, 15–24 (2002).
9. E. R. Dufresne and D. G. Grier, "Optical tweezer arrays and optical substrates created with diffractive optical elements," *Rev. Sci. Instrum.* **69**, 1974–1977 (1998).
10. D. G. Grier, "A revolution in optical manipulation," *Nature (London)* **424**, 810–816 (2003).
11. A. Rohrbach and E. H. K. Stelzer, "Trapping forces, force constants, and potential depths for dielectric spheres in the presence of spherical aberrations," *Appl. Opt.* **41**, 2494–2507 (2002).
12. M. Capitanio, G. Romano, R. Ballerini, M. Giuntini, F. S. Pavone, D. Dunlap, and L. Finzi, "Calibration of optical tweezers with differential interference contrast signals," *Rev. Sci. Instrum.* **73**, 1687–1696 (2002).
13. K. Berg-Sorensen and H. Flyvbjerg, "Power spectrum analysis for optical tweezers," *Rev. Sci. Instrum.* **75**, 594–612 (2004).

14. M. Klein, M. Andersson, O. Axner, and E. Fallman, "Dual-trap technique for reduction of low-frequency noise in force measuring optical tweezers," *Appl. Opt.* **46**, 405–412 (2007).
15. H. Faxen, "Die Bewegung einer starren Kugel langs der Achse eines mit zäher Flüssigkeit gefüllten Rohres," *Ark. Mat. Astron. Fys* **17**, 1–28 (1923).
16. S. Keen, J. Leach, G. Gibson, and M. J. Padgett, "Comparison of a high-speed camera and a quadrant detector for measuring displacements in optical tweezers," *J. Opt. A, Pure Appl. Opt.* **9**, S264–S266 (2007).
17. W. Singer, S. Bernet, N. Hecker, and M. Ritsch-Marte, "Three-dimensional force calibration of optical tweezers," *J. Mod. Opt.* **47**, 2921–2931 (2000).
18. Y. K. Nahmias, B. Zhi Gao, and D. J. Odde, "Dimensionless parameters for the design of optical traps and laser guidance systems," *Appl. Opt.* **43**, 3999–4006 (2004).
19. F. Belloni and S. Monneret, "Quadrant kinoform: an approach to multiplane dynamic three-dimensional holographic trapping," *Appl. Opt.* **46**, 4587–4593 (2007).
20. S. Monneret, F. Belloni, and O. Soppera, "Combining fluidic reservoirs and optical tweezers to control beads/living cells contacts," *Microfluid. Nanofluid.* (2007).

1. Introduction

Optical forces have a long history of experimental evidences and theoretical calculations behind; nevertheless the actual measurements have always proven to be difficult if not prohibitive in many conditions. Since the first observations of Kepler in the early 17th century, scientists have struggled to quantify the effects of light on matter. The first experimental data came only at the beginning of the last century from the work of a Russian physicist, Lebedev [1]. The introduction of Optical Tweezers (OT) [2] produced quite a revolution, since the range of optical forces that could be exerted became suddenly more important and therefore more suitable for experimental measurements.

The importance of OT force calibration is twofold: on one side it verifies the predictions from the theory, on the other it allows to investigate small forces phenomena in a contactless manner. In the latter scenario calibrated OT can act as sensors to detect and measure forces generated by the system under observation. In an opposite fashion, calibrated OT can act as actuators to impart precise forces on the sample, such as red blood cells [3]. With these motivations, parallel to the development of OT setups ran the development of calibration techniques the aim of which was to quantify the actual interaction between light and matter. Several of these techniques are now standard in the field and can lead to extremely accurate measurements of forces ranging down from piconewtons to femtonewtons, [4, 5, 6]. However, all such techniques, except the original one described in [7], have been implemented in restricted configurations of one or two traps, and especially on the assumption that the traps were isotropic in force. In this paper, we would like to report the extension to a multi-axes exploration of the potential well reconstruction method against drag force [8] to simultaneously characterize the potential wells of several trapping sites generated with Holographic Optical Tweezers (HOT) [9, 10]. The final result is a robust, fast and automatic procedure we use to highlight specific properties of HOT. This article mainly describes the method, focusing on its reliability and its application to address the dependence of the diffraction efficiency with the trap position in a given traps pattern. In a second forthcoming paper, we will use the method in its 6-axes configuration to demonstrate how optical aberrations and/or mutual interactions between holographic traps can create distorted potential energy landscapes around the traps in a holographic traps pattern.

2. Force calibration

From the theory we know that the force exerted on a homogeneous sphere by an optical trap presents a general non linear behaviour with respect to the spatial coordinates [11]. However, for small displacements from the equilibrium we can assume the linear model of a spring which directly relates the displacement of the trapped object to the exerted force. Therefore, the characterization of the spring stiffness, in conjunction with the quantification of the displacement

from the centre of the trap, will provide the instantaneous force on the trapped object. It is important to understand that we can not retrieve the maximum force a trap can exert from the spring model as, “the escape velocity [i.e. the maximum force] in fact is due to the anharmonicity of the trap, while the stiffness comes out from the harmonic approximation near the trap center”, as pointed out in [12]. It is important to note also that these forces depend strongly on the nature of the trapped object both in terms of object morphology and composition; therefore it is mandatory to fix convenient working conditions in order to be able to reproduce the measurements. Traditionally this is achieved using well characterized micrometric spheres.

The power spectrum method, based on the harmonic approximation, probably provides the most accurate results. It relies on the analysis of the Brownian fluctuations of a trapped bead which are related to a Lorentzian fit. The fitting, together with the knowledge of some experimental parameters, directly provides the value of the trap stiffness which can then be related to the instantaneous force exerted by the trap [13]. However, the high accuracy of the method is counterbalanced by the setup configuration which limits the number of traps that can be calibrated at the same time; literature reports up to two traps calibrated simultaneously [14].

A more recent technique has been proposed by Polin et al. [7] and allowed them to calibrate 119 colloidal spheres simultaneously, along two orthogonal lateral axes of the traps, through digital video microscopy combined with an optimal statistical analysis of each of the spheres' thermally driven motions.

2.1. Potential well characterization theory

The potential well reconstruction method, described in [8], also relies on the harmonic approximation of the optical trap where the force exerted is much weaker than the maximum exertable force. According to this model, the Hooke law defined as

$$F_{spring}(r) = -k \cdot r \quad (1)$$

expresses the linear relationship between the deformation r of the equivalent spring and the force F_{spring} required to obtain such a deformation. k is commonly called the stiffness of the trap. It is well known that such a force is conservative and therefore we can define its potential as

$$U_{spring}(r) = \frac{1}{2}k \cdot r^2 = \frac{1}{2}F_{spring}r \quad (2)$$

The potential well reconstruction technique simply consists in quantifying the displacement of a trapped bead from its equilibrium position when a known force is applied and retrieve the trap stiffness performing a linear or parabolic fitting respectively on Eq. 1 or Eq. 2. In the case of a perfectly isotropic potential, the retrieved k characterizes the whole potential. From a different point of view, we can think of the procedure as if we inject some energy in the system and then observe the trapped object climbing up the walls of the potential well to the corresponding energy level. As a consequence, this method should allow to probe anisotropic or distorted potential wells, by simply recording the successive equilibrium positions of trapped beads when the direction of the external driving force is changed.

3. Calibration method

The trapping is achieved via a 2W near infrared laser at $\lambda = 1052\text{nm}$ (IPG Laser, Germany) and the procedure implemented is the following one: we move the immersion fluid (deionized water), of given viscosity, by two orthogonally mounted motorized stages (Physik Instrumente. M-126CG with C843 controllers), which are speed and acceleration calibrated for movements down to a theoretical step size of 3.5nm with maximum speed of $600\mu\text{m/s}$. Assuming a laminar flow, this results in the application of a uniform calibrated drag force on all the trapped beads.

This drag force is given by Stokes equation, and can be corrected to take into account the effects of a close coverslip [15]. The movements are performed several times for several different speeds to accumulate many data points for each energy level and increase the reliability of the fitting. The movements are also repeated along several axes in the two opposite directions in order to analyze anisotropies in the potential wells, i.e. different displacements from the equilibrium for the same modulus of applied force but along different directions. In this paper, only two orthogonal axes, noted X and Y, are considered. The positions of all the trapped objects are retrieved by image processing. In order to obtain the best performances from our tracking algorithm we decided to use fluorescent homogeneous beads (Dragon Green Polystyrene fluorescent beads from Bangs Laboratories, diameter of 3.69 μm with a standard deviation of 0.34 μm , density of 1.067 g/cm^3), and work with the fluorescence imaging of the microscope. In such a way, the recorded images are physically thresholded to be black and white and the algorithm is faster and more accurate. The image acquisitions are performed with a custom made time-lapse software interfaced with the UV lamp shutter, a standard videosurveillance camera (WAT-902B, Watec), digitalization and storing on hard drive with a frame grabber at 12fps, 768 \times 576 pixels resolution (Picolo Industrial, Euresys). Finally, for a high signal to noise ratio it is advisable for each bead to cover as much pixels as possible on the final image; to maximize this parameter we worked with a high magnification objective (Nikon Plan Fluor 100 \times , NA = 1.3, oil immersion, plus an additional 1.5 magnification that is accessible on our Nikon TE 2000U microscope). See Fig. 1 for a scheme of the procedure.

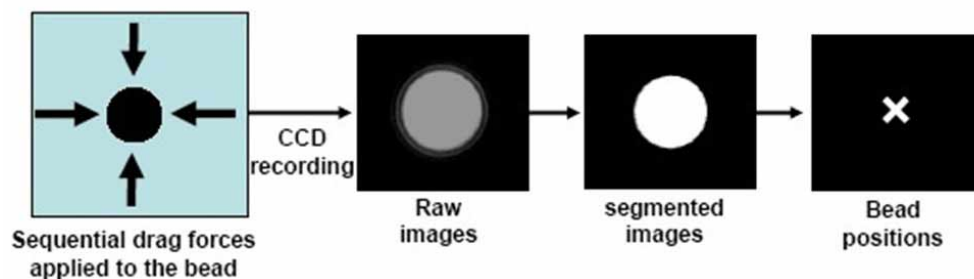


Fig. 1. Calibration technique basic steps. (a) Uniform speed motions are applied along two orthogonal axes in four different directions imparting a calibrated drag force onto the trapped object; (b) Time-Lapse fluorescent imaging provides a stack of raw images where we select one or more regions of interest; (c) Matlab tracking algorithm performs an image segmentation and (d) evaluates the position of the bead center.

The main advantage of this technique is given by the possibility to repeat several times the calibration with the same trapped bead and therefore avoid uncertainties linked to the beads polydispersity. Moreover, repeatability without any user interaction has been exploited to obtain a reliable automatic procedure. The downside is represented by the need for an accurate position detecting system, that can be either software, based on image processing like in our case, or hardware like a quadrant photodiode, the latter being the most accurate but limited in the number of configurations it can be used with.

3.1. Algorithm calibration

Since the images are physically thresholded, the tracking algorithm implemented in Matlab (The Mathworks, Natick, MA) is straightforward and consists of a simple image segmentation followed by a barycenter calculation. Nevertheless, a calibration is necessary to retrieve the accuracy we can attain for beads displacements from the equilibrium position. The assay de-

vised to quantify this parameter consisted in the position tracking of a single bead attached to the coverslip when a stepped translation along the x axis was performed. The motorized linear stages we dispose of are calibrated at the factory and we assumed no errors in operations. However, despite the minimum theoretical step size of 3.5nm we found that the minimum accurate displacement was in steps of ten base units, therefore 35nm. The captured images were subsequently processed by the tracking algorithm that produced the plot reported in Fig. 2. We can see how the algorithm performs definitely better than the 35nm resolution achievable with the motorized stages, despite some spikes in the transient regions probably due to the prompt acceleration. We recalibrated the algorithm with acquisitions obtained via a piezo-electric position stage and found the resolution limit to be in the range of ten nanometres (plot not shown), which is comparable with data reported in [7, 16].

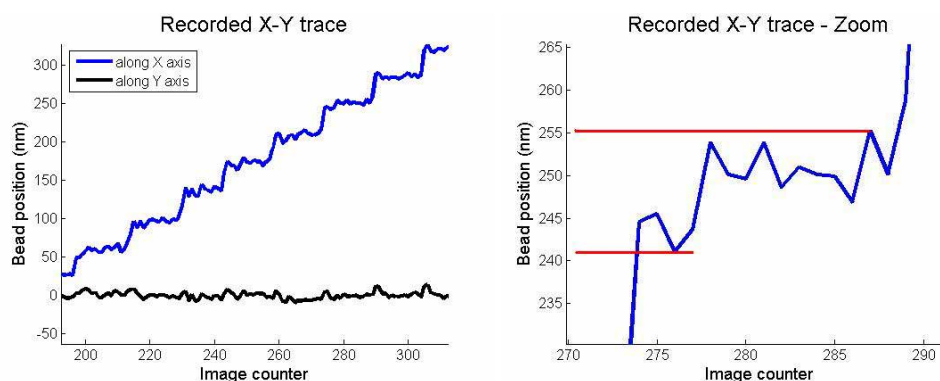


Fig. 2. Tracking algorithm calibration. Left, the position of a bead attached to the coverslip is tracked when the stage translates along the x axis in steps of 35nm. Right, a zoom shows the algorithm accuracy to be approximately ten nanometers

3.2. Output

The tracking algorithm provides the positions of each bead in a selected region of interest for all the successive images of the recorded stack; for a given bead these values generate two plots: the scattering plot of the x, y bead coordinates, see Fig. 3 left and the x, y split coordinates versus the image counter, i.e. time, see Fig. 4 left. The first outcome of the scattering plot is the verification of the correct alignment of the motorized stage with the image acquisition system; in case of misalignment, the axes of the plotted cross would not be orthogonal. This plot is also representative of the explored energy levels of the optical potential well and can be represented by a contour line as depicted in Fig. 3 right, where each isocurve corresponds to a specific energy level that we reach imparting an increasing drag force (black arrows in the plot). The second diagram, which we call “trace” of a bead, reports the selected bead coordinates versus the image counter, see Fig. 4 left. To each peak corresponds a displacement of the trapped bead from the equilibrium according to the imparted drag force; we can note the six repetitions for each velocity and five different velocities to accumulate many data points for a reliable fit. It should be also noted that the number of points in each maximum depends on the distance travelled at uniform velocity; usually tens of points per maximum are taken. This plot is useful to verify the absence of impulsive external perturbations such as a mechanical vibration or a segmentation error in the tracking software due to noise in the image. All of these effects can invalidate the experiment, hence the importance of this test. The processing of the whole trace extracts the values of the equilibrium positions, i.e. the average of the points in the local

maxima, of a bead under the action of varying drag force (black dots in Fig. 4 left), or in different terms the equilibrium positions of a bead climbing the optical potential well when a certain energy is imparted, the same points are plotted in Fig. 3 right. Finally, the software performs a linear regression on the averaged peak values and automatically evaluate the trap stiffness, see Fig. 4 right. Please note that we chose to fit data to Eq. 1 because a parabolic fit would have lost the directional anisotropy for displacements lying on the same axis.

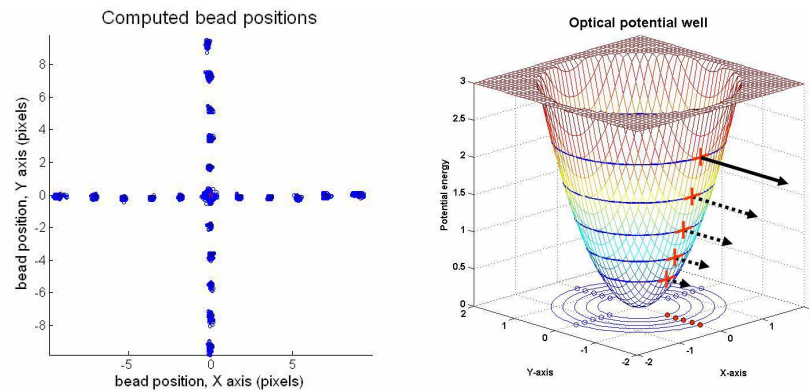


Fig. 3. Algorithm output 1. Left, the scattering plot of the x, y bead coordinates evaluated by the image processing algorithm. Right, the conceptual image of a trapped bead climbing up the walls of a potential well as the result of an imparted external force, in our case a calibrated drag force represented by the black arrows.

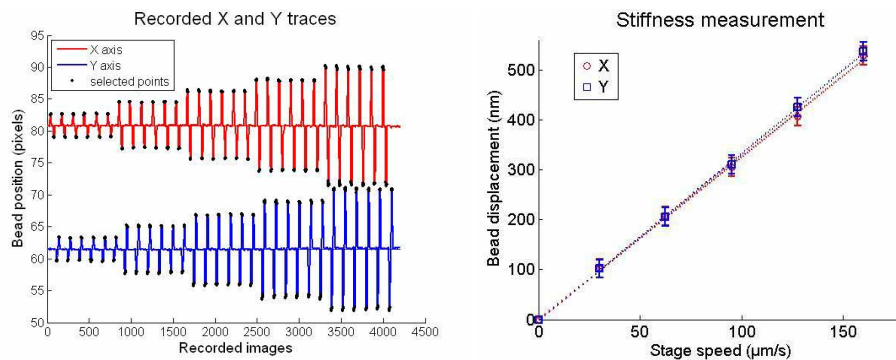


Fig. 4. Algorithm output 2. Left, the x, y bead coordinates are plotted separately versus the image counter, i.e. time. The black dots show the selected values, usually tens per peak, which are averaged to extract the equilibrium position corresponding to a specific drag force. This mean values are then used to perform a linear regression and extract the stiffness of the selected trap, right figure.

The precision on the absolute stiffness value is approximately 18% and takes into account the contribution from beads parameters (9%), temperature and medium viscosity (4%), linear regression on beads position (1%) and distance from the coverslip (4%). On the other hand, the reliability of the procedure is particularly adapted to relative measurements, as it is the case in our applications. In order to prove it we repeated five times the calibration procedure on the same trapped bead for a fixed power of 43mW at the sample, with a reduced number of acquisitions (three repetitions for each of the three different speeds) and we found the trap

stiffness to vary in the range $k_x = 12.54 \cdot 10^{-6} \text{ N/m} \pm 1.3\%$ and $k_y = 12.84 \cdot 10^{-6} \text{ N/m} \pm 0.5\%$ respectively along the x and y axes.

The last test we employed to verify the reliability of the calibration procedure analyzes the relationship between the trap stiffness and the laser power at the trap, which from the theory we know to be linear. Moreover, we exploited the parallelism of the image processing to analyze two traps at the same time: on one side a bead is blocked within an holographic trap, on the other, a bead is trapped within the zero order of our reconstruction, see Fig. 5. The results are in agreement with theory (linear fit), and in agreement with previous experiments for comparable beads materials and power levels, [7, 12, 17, 18]. Please note that the power is here shared between two traps and therefore for a comparison with results in literature we need to take it into account.

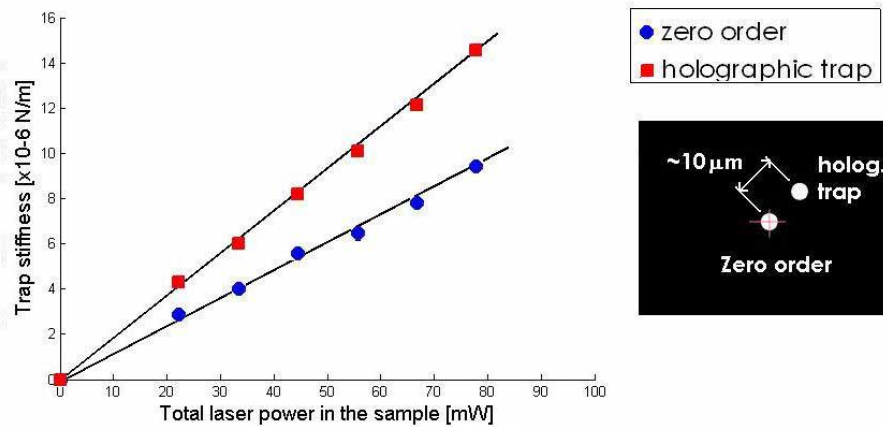


Fig. 5. Left, trap stiffness versus the total laser power in the sample, for two beads trapped simultaneously. Right the traps pattern used during the experiment. Distance to coverslip is $10\mu\text{m}$.

4. Applications

The diffraction efficiency of spatial light modulators (SLMs) is a fundamental parameter in holographic trapping. This value tells us the amount of light which is going to be diverted in the desired reconstruction with respect to the hologram spatial frequency content. The farther the reconstruction is from the optical axis, the most important the high spatial frequency content of the hologram and as a consequence, the lower diffraction efficiency and trap stiffness. Therefore, the stiffness of a trap is a function of its position within the reconstruction volume. We here report an analysis of the position dependence of the stiffness of an holographic trap. It is important to underline how this parameter depends on the resolution of the SLM employed to modulate the laser wavefront; hence, the following results are strictly related to our setup and SLM (Hamamatsu X8267-15, see [19] for details on the setup). The results are reported in Fig. 6.

We can now exploit the parallelism offered by our calibration method and simultaneously analyze multiple traps at different distances from the optical axis as reported in Fig. 7. Once again the results of the calibration confirm what reported in Fig. 6. This calibration offers an interesting perspective application to obtain an homogeneous reconstruction; we can think of inverting this relation and compensate the diffraction losses enhancing the farthest traps in the field of view with exactly the required amount of power.

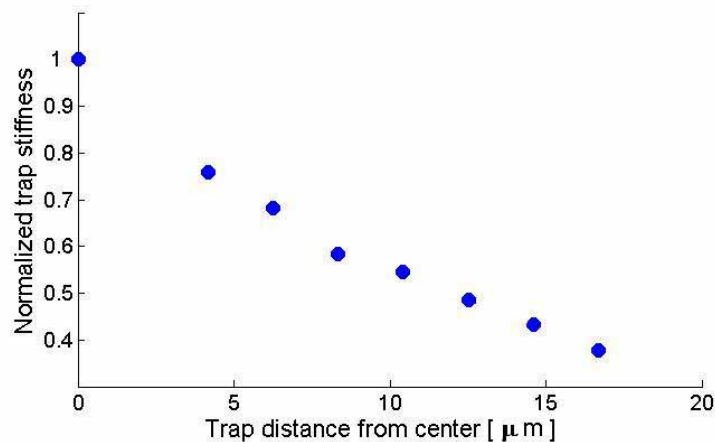


Fig. 6. The normalized stiffness of an holographic trap is reported as a function of the distance with respect to the zero order. Distance to coverslip is $10\mu\text{m}$.

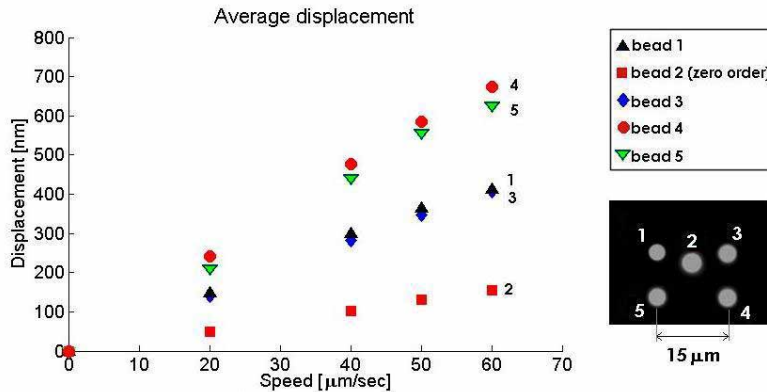


Fig. 7. Multiple trap characterization. Left, the trap stiffness mainly depends on the trap position relative to the optical axis, or zero order (bead 2), because of variations in the diffraction efficiency. Right the traps pattern used during the experiment. Distance to coverslip is $10\mu\text{m}$.

The possibility to reliably characterize multiple traps in a short time really opens new perspective and the applications are several. An interesting one is the characterization of ghost traps in HOT. Everybody is familiar with the generally annoying presence of residual diffraction orders that can interfere with the desired traps or eventually become traps themselves. We decided to quantify such ghost traps with the idea of deriving information about the quality of the algorithm that generates the hologram. The experiment consisted in generating a single holographic trap with a simple algorithm [19], which provided enough light to trap in the zero and -1 orders as well. A picture of the traps pattern is reported in Fig. 8 while the results of the characterization are reported in Table 4. The whole characterization took less than three minutes total time: fifty seconds acquisitions plus forty seconds of software processing for each bead.

The apparent difference in the diameters of the beads in Figs. 7 and 8 comes mainly from a

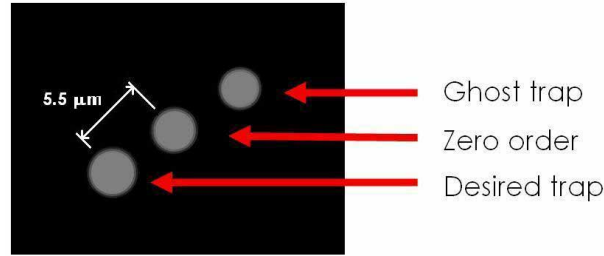


Fig. 8. Ghost traps characterization. The distance of the first order from the center is $\approx 5.5\mu\text{m}$.

Table 1. Characterization of an holographic trap and its residual diffraction orders.

Stiffness [$k \cdot 10^6\text{N/m}$ @ $P=67\text{mW}$]	Desired trap	Zero order	Ghost trap
k_x	11.45	4.7	2.95
k_y	11.9	4.2	2.15

difference in the fluorescence level of the beads associated with a saturated image which gives the required physical threshold for our tracking algorithm, and not from a large difference in the beads diameters themselves.

5. Preventing collisions

To enhance the accuracy we need to increase the duration of the fluid motion in order to obtain more samples. This in turn increases the chances of stray beads colliding with the trapped ones. On the other hand working with low bead concentration is not advisable if the goal is to perform a parallel calibration of multiple beads, too much time would be spent looking for beads. We therefore combined our sample with isolation chambers built with a microstereolithographic process that only contains the beads we trapped as depicted in Fig. 9, see [20] for details on microstereolithography. This procedure allowed us to perform accurate experiments several times on the same bead and eventually replace it when too much photobleaching occurs. Moreover, isolation chambers shield the trapped beads from external fluxes which might be present outside and that could cause a distortion in the cross diagrams.

6. Conclusions and perspectives

The calibration method we developed extends the principle described in [8] to the parallel calibration of multiple traps. The method based on image processing and calibrated displacement of the sample proves to be reliable, fast and easy to implement. The applications are several and we here report some related to the characterization of HOT since this is the technique we use for multiplying the trapping sites; nevertheless the method can be applied to any multiple traps technique for characterization. Here we were able to characterize the effects of SLM diffraction efficiency on traps stiffness and to quantify the magnitude of ghost traps; we limited ourselves to a single algorithm but in perspective we think of performing a quantitative parametric study of different algorithms with different diffractive optical elements (DOE) characteristics. Other applications will be described in a forthcoming paper; they concern the fine multi-axes characterization of distorted optical potential wells of holographic optical traps, where distortion comes from optical aberration and/or effects due to nearby ghost or regular traps.

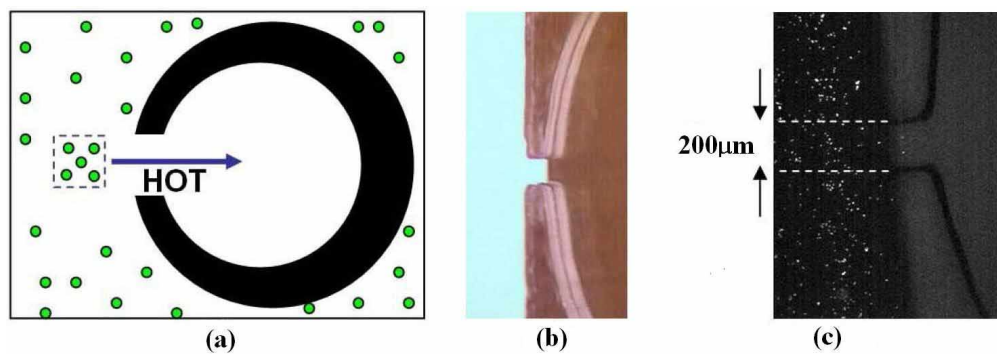


Fig. 9. (a) Principle of beads confinement. (b) Picture of the chamber with detail of the entrance. (c) Picture taken in working conditions but with a 4X objective, low white light to see the microstereolitographic structure and fluorescence light to image the beads confined outside the chamber.